

# Heterogeneity of Collagen VI Microfibrils

## STRUCTURAL ANALYSIS OF NON-COLLAGENOUS REGIONS\*

Received for publication, November 18, 2015, and in revised form, December 23, 2015. Published, JBC Papers in Press, January 7, 2016, DOI 10.1074/jbc.M115.705160

Tobias Maaß<sup>‡</sup>, Christopher P. Bayley<sup>§</sup>, Matthias Mörgelin<sup>¶</sup>, Sandra Lettmann<sup>‡</sup>, Paolo Bonaldo<sup>||</sup>,  
Mats Paulsson<sup>†\*\*\*§§</sup>, Clair Baldock<sup>§1,2</sup>, and Raimund Wagener<sup>†\*\*\*1,3</sup>

From the <sup>‡</sup>Center for Biochemistry, Medical Faculty, <sup>\*\*</sup>Center for Molecular Medicine, <sup>\*\*</sup>Cologne Excellence Cluster on Cellular Stress Responses in Aging-associated Diseases, and <sup>§§</sup>Center for Musculoskeletal Biomechanics, University of Cologne, D-50931 Cologne, Germany, the <sup>§</sup>Wellcome Trust Centre for Cell-Matrix Research, University of Manchester, Manchester M13 9PT, United Kingdom, the <sup>¶</sup>Department of Clinical Sciences, Division of Infection Medicine, Lund University, SE-221 84 Lund, Sweden, and the <sup>||</sup>Department of Molecular Medicine, University of Padova, 35131 Padova, Italy

Collagen VI, a collagen with uncharacteristically large N- and C-terminal non-collagenous regions, forms a distinct microfibrillar network in most connective tissues. It was long considered to consist of three genetically distinct  $\alpha$  chains ( $\alpha 1$ ,  $\alpha 2$ , and  $\alpha 3$ ). Intracellularly, heterotrimeric molecules associate to form dimers and tetramers, which are then secreted and assembled to microfibrils. The identification of three novel long collagen VI  $\alpha$  chains,  $\alpha 4$ ,  $\alpha 5$ , and  $\alpha 6$ , led to the question if and how these may substitute for the long  $\alpha 3$  chain in collagen VI assembly. Here, we studied structural features of the novel long chains and analyzed the assembly of these into tetramers and microfibrils. N- and C-terminal globular regions of collagen VI were recombinantly expressed and studied by small angle x-ray scattering (SAXS). *Ab initio* models of the N-terminal globular regions of the  $\alpha 4$ ,  $\alpha 5$ , and  $\alpha 6$  chains showed a C-shaped structure similar to that found for the  $\alpha 3$  chain. Single particle EM nanostructure of the N-terminal globular region of the  $\alpha 4$  chain confirmed the C-shaped structure revealed by SAXS. Immuno-EM of collagen VI extracted from tissue revealed that like the  $\alpha 3$  chain the novel long chains assemble to homotetramers that are incorporated into mixed microfibrils. Moreover, SAXS models of the C-terminal globular regions of the  $\alpha 1$ ,  $\alpha 2$ ,  $\alpha 4$ , and  $\alpha 6$  chains were generated. Interestingly, the  $\alpha 1$ ,  $\alpha 2$ , and  $\alpha 4$  C-terminal globular regions dimerize. These self-interactions may play a role in tetramer formation.

Collagen VI is a widely expressed member of the triple helix-containing protein superfamily of collagens (1). In contrast to

the abundant fibril-forming collagens I and II, collagen VI forms beaded microfibrils that anchor large interstitial structures (2). Other extracellular matrix proteins bind to the non-collagenous domains and are important for the embedding of these microfibrils in the matrix (3–6). Collagen VI has the lowest triple helix content among all collagens and is predominantly composed of globular VWA<sup>4</sup> domains (7).

For many years collagen VI was thought to consist of only the shorter  $\alpha 1$  and  $\alpha 2$  chains and the longer  $\alpha 3$  chain. Intracellularly, heterotrimeric monomers are formed that assemble to dimers in an antiparallel fashion. These subsequently assemble laterally to tetramers, are secreted, and finally associate end to end to form beaded microfibrils (Fig. 1) (8, 9). More recently, three novel long chains,  $\alpha 4$ ,  $\alpha 5$ , and  $\alpha 6$ , were identified (Fig. 1) that are thought to substitute for the  $\alpha 3$  chain in the assembly (10, 11). Interestingly, humans and modern apes lost the  $\alpha 4$  chain by a large pericentral inversion on chromosome 3 (12). The novel long chains have a restricted, often complementary expression at certain basement membranes (13).

Mutations in the  $\alpha 1$ ,  $\alpha 2$ , and  $\alpha 3$  chains cause collagen VI-related myopathies (14) ranging from the severe Ullrich congenital muscular dystrophy to the milder Bethlem myopathy, including intermediate forms (15). Mutations in the  $\alpha 1$  and  $\alpha 2$  chains can also lead to limb-girdle muscular dystrophy (16) and a mutation in the  $\alpha 2$  chain to myosclerosis (17). Recently, early onset isolated dystonia, a neurological disease, was shown to be caused by mutations in the  $\alpha 3$  chain (18). Interestingly, a possibly digenic myopathy patient carried compound heterozygous mutations in the  $\alpha 6$  chain and a mutation in the  $\alpha 3$  chain (19).

Collagen VI  $\alpha 1$  knock-out mice that develop a mild form of myopathy (20) were used for in depth studies of the myopathy pathomechanism. The muscles of the knock-out mice lose their contractile strength and display a marked dilation of the sarcoplasmic reticulum. Abnormal mitochondria are seen in muscle cells, with altered cristae and dense bodies and an opening of the mitochondrial permeability transition pore leading to enhanced apoptosis (21). The persistence of abnormal mitochondria and apoptosis is caused by a disturbed autophagy (22). Moreover, the mice show impaired muscle regeneration and

\* This work was supported in part by Deutsche Forschungsgemeinschaft Grant SFB829/B2 (to the R. W. and M. P. laboratories), Biotechnology and Biological Sciences Research Council Grant BB/I012265/1 (to C. B.), Boehringer Ingelheim Fonds (to T. M.), Swedish Research Council Project 7480, the Swedish Foundation for Strategic Research, the Foundations of Crafoord, Johan and Greta Kock, Alfred Österlund, King Gustav V Memorial Fund, and the Medical Faculty at Lund University. The authors declare that they have no conflicts of interest with the contents of this article.

✂ Author's Choice—Final version free via Creative Commons CC-BY license.

<sup>1</sup> Both authors contributed equally to this work.

<sup>2</sup> To whom correspondence may be addressed: Wellcome Trust Centre for Cell-Matrix Research and Faculty of Life Sciences, University of Manchester, Manchester M13 9PT, United Kingdom. Tel.: 44-161-2755439; Fax: 44-161-2755082; E-mail address: clair.baldock@manchester.ac.uk.

<sup>3</sup> To whom correspondence may be addressed: Institute for Biochemistry II, Medical Faculty, University of Cologne, 50931 Cologne, Germany. Tel.: 49-221-4786990; Fax: 49-221-4786977; E-mail: raimund.wagener@uni-koeln.de.

<sup>4</sup> The abbreviations used are: VWA, von Willebrand factor type A domain; SAXS, small-angle x-ray scattering; EOM, ensemble optimization method.

## Heterogeneity of Collagen VI Microfibrils

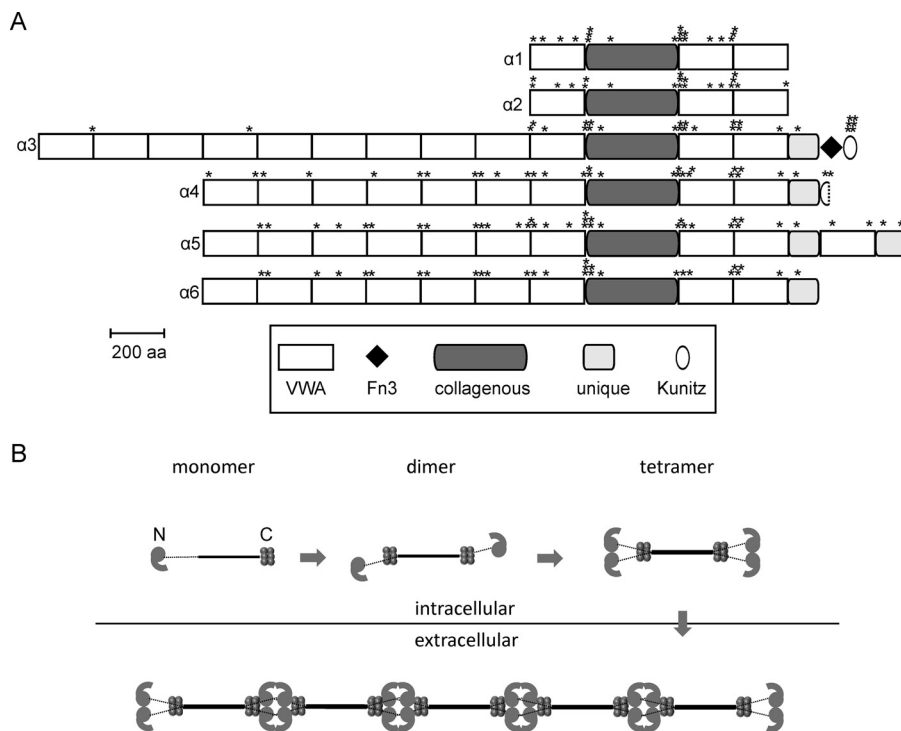


FIGURE 1. **Domain structure (A) and assembly (B) of collagen VI chains.** A, positions of the cysteine residues are marked by *asterisks* above each chain. The domain structure is as shown in Ref. 50. VWA, von Willebrand factor type A domain, Fn3, Fibronectin type 3 domain. B, intracellularly the heterotrimeric monomers assemble to tetramers that are secreted and form microfibrils in the extracellular space. Adapted from Ref. 24.

**TABLE 1**  
Primers for expression constructs

The following abbreviations are used: fw, forward; rev, reverse. The restriction enzyme recognition sites are underlined.

Chain	5'–3' Sequence	Restriction enzyme
$\alpha$ 3N	tatctcgagctgatggatctgctgtgaggta (fw)	XhoI
	aggaaccagggatcccaggggcctgtcatacatgaagcc (rev)	BamHI
$\alpha$ 4N	attgctagcccacagagattgtctcgaggaggcgtctg (fw)	NheI
	aggctcgagcagtaagacgcttggagg (rev)	XhoI
$\alpha$ 5N	attgctagccttagaccagagcccagggccaggccccagta (fw)	NheI
	atactcgaggagcgtcttggcccaggtctagcatcccattgg (rev)	XhoI
$\alpha$ 6N	attgctagccaagattctggccccaggtacgcagac (fw)	NheI
	tatctcgagcagctgactcccagggttcc (rev)	XhoI
$\alpha$ 1C	gcagctagctgcacatgtggaccattga (fw)	NheI
	aacctcgaggcccagtgccaccttct (rev)	XhoI
$\alpha$ 2C	gaagctagctgtgagaagcgtgtgt (fw)	NheI
	gcaggatccacagatccagcggatg (rev)	BamHI
$\alpha$ 3C	aaagctagcctggagtgccctgtattcccac (fw)	NheI
	tttggatcctcaactgttaactcaggactac (rev)	BamHI
$\alpha$ 4C	attgctagcggatattccaggtgccag (fw)	NheI
	agcggatcccttcaagacataattcaggc (rev)	BamHI
$\alpha$ 5C	attgctagcgacaagtgccctgtgtatcc (fw)	NheI
	agcggatcctcttgcctcttgcctcctt (rev)	BamHI
$\alpha$ 6C	attgctagcggaaaactcagtgccagc (fw)	NheI
	agcggatccggcactctgtttaccaggttt (rev)	BamHI

reduced satellite cell self-renewal after injury (23). However, little is known about the structural consequences of patient mutations that do not affect the formation of the triple helix.

The structure of the non-collagenous parts of collagen VI has mainly been studied by use of electron microscopy. Moreover, by SAXS it was shown that the extended array (N9 to N1) of N-terminal VWA domains of the  $\alpha$ 3 chain has a tight C-shape. Indeed, in collagen VI bead regions, the N-terminal globules predominantly consisting of  $\alpha$ 3 chain VWA domains project out from the globular bead region like angled radial spokes. These could potentially provide interaction surfaces for other cell surface or matrix molecules (24). Only two collagen VI

**TABLE 2**  
SAXS values

NSD is normalized spatial discrepancy. ND means not determined.

Construct	DAMMIN $\chi$ range	Damsel NSD	SASREF $\chi$ range
$\alpha$ 1C	1.366–1.380	0.88	1.16–1.21
$\alpha$ 2C	0.879–0.887	0.80	0.74–0.97
$\alpha$ 4N	0.718–0.793	0.74	1.09–1.10
$\alpha$ 4C	1.025–1.028	0.69	ND
$\alpha$ 5N	1.063–1.089	0.78	ND
$\alpha$ 6N	0.604–0.610	0.81	ND
$\alpha$ 6C	1.187–1.196	0.66	ND

domain structures have been resolved to high resolution, the Kunitz domain (25) and the N5 VWA domain of the  $\alpha$ 3 chain (26). The latter structure showed that in contrast to VWA domains in other proteins, a C-terminal extension is present that places the N and C termini at opposite sides of the globular domains. This allows a near-linear arrangement of the adjacent VWA domains and is in good agreement with the SAXS model of the N9 to N1 fragment of the  $\alpha$ 3 chain. As a consequence of the sparse structural information, only few aspects of the complex assembly are understood at atomic resolution. It was proposed that alternating hydrophobic and ionic interactions between the antiparallel triple helices (27) and interactions between the triple helix and the C2 domain of the  $\alpha$ 2 chain are important for dimer formation (28). Moreover, it was shown that at least the N5 to N1 domains of the  $\alpha$ 3 chain are important for the microfibril formation (29) and that the Kunitz domain can be cleaved off immediately after fibril formation (30). Studies on the impact of mutations found in myopathy patients also gave insight into the role of different domains, e.g. the critical importance of a correctly folded C1 domain of the collagen VI  $\alpha$ 2 chain in microfibril formation (31).

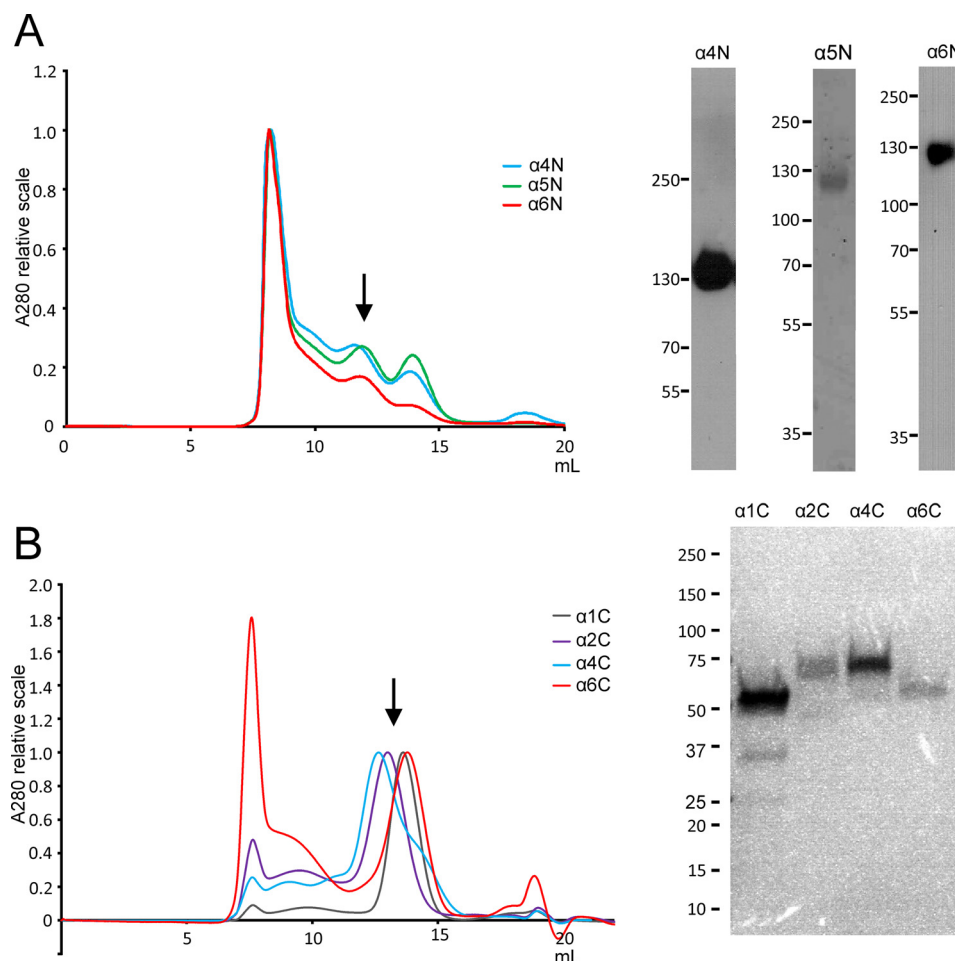


FIGURE 2. Purification of recombinant N-terminal (A) and C-terminal (B) regions of collagen VI  $\alpha 1$ ,  $\alpha 2$ ,  $\alpha 4$ ,  $\alpha 5$ , and  $\alpha 6$  chains. Left side, size-exclusion chromatography (example runs are shown) was performed to further purify the protein samples that were obtained after affinity purification and to remove higher aggregates. Absorption was normalized for the main peaks of the different chromatograms. Collected fractions are indicated by arrows. Right side, purity of the fractions was evaluated by SDS-PAGE and subsequent Ponceau staining ( $\alpha 5$  chain) (A) or Western blotting ( $\alpha 4$  and  $\alpha 6$  chain) using chain-specific antibodies (A) or Coomassie staining (B).

Nevertheless, most aspects of structure and assembly of collagen VI and especially of the contribution of the novel long chains are not known. Which are the spatial structures of their non-triple helical parts? Do they assemble into tetramers, as has been shown for collagen VI molecules containing the  $\alpha 3$  chain? How are they involved in fibril formation? We therefore performed a comprehensive study to determine structures within the novel long chains and to analyze the composition and assembly of  $\alpha 4$ ,  $\alpha 5$ , and  $\alpha 6$  chains containing collagen VI tetramers and microfibrils.

### Experimental Procedures

**Recombinant Expression and Purification of N- and C-terminal Domains of Collagen VI  $\alpha$  Chains and Generation of Specific Antibodies**—The cDNA constructs coding for the non-collagenous domains of collagen VI were generated by RT-PCR on total RNA from brain or intestine and cloned with 5'-terminal NheI or XhoI and 3'-terminal BamHI or XhoI restriction sites (Table 1). Each of the amplified PCR products were inserted into a modified pCEP-Pu vector containing an N-terminal BM-40 signal peptide and a C-terminal One-STREP tag downstream of the restriction sites (32). HEK293-EBNA cells (Invit-

rogen) were transfected with the recombinant plasmids using the FuGENE 6 reagent (Roche Applied Science, Mannheim, Germany) according to the manufacturer's protocol. The cells were selected with puromycin (1  $\mu$ g/ml), and the recombinant proteins were purified directly from serum-containing cell culture medium. After filtration and centrifugation (1 h, 10,000  $\times$  g), the cell culture supernatants were applied to a StrepTactin column (1.5 ml, IBA GmbH) and eluted with 2.5 mM desthiobiotin, 10 mM Tris-HCl, pH 8.0. The purified recombinant C-terminal collagen VI fragments were used to immunize rabbits. To abolish cross-reactivity, the antisera were depleted on columns coupled with all other N- and C-terminal fragments and specific antibodies purified by affinity chromatography on a column with antigen coupled to CNBr-activated Sepharose (GE Healthcare). The specific antibodies were eluted with 0.1 M glycine, pH 2.5, and the eluate was neutralized with 1 M Tris-HCl, pH 8.8, and adjusted to 150 mM NaCl.

**Gel Electrophoresis and Immunoblot**—Collagen VI was purified from whole newborn mouse carcasses as described (33). Samples were subjected to SDS-PAGE on 8% (w/v) polyacrylamide gels under reducing conditions (5%  $\beta$ -mercaptoethanol). Proteins were electrophoretically transferred to Immo-

## Heterogeneity of Collagen VI Microfibrils

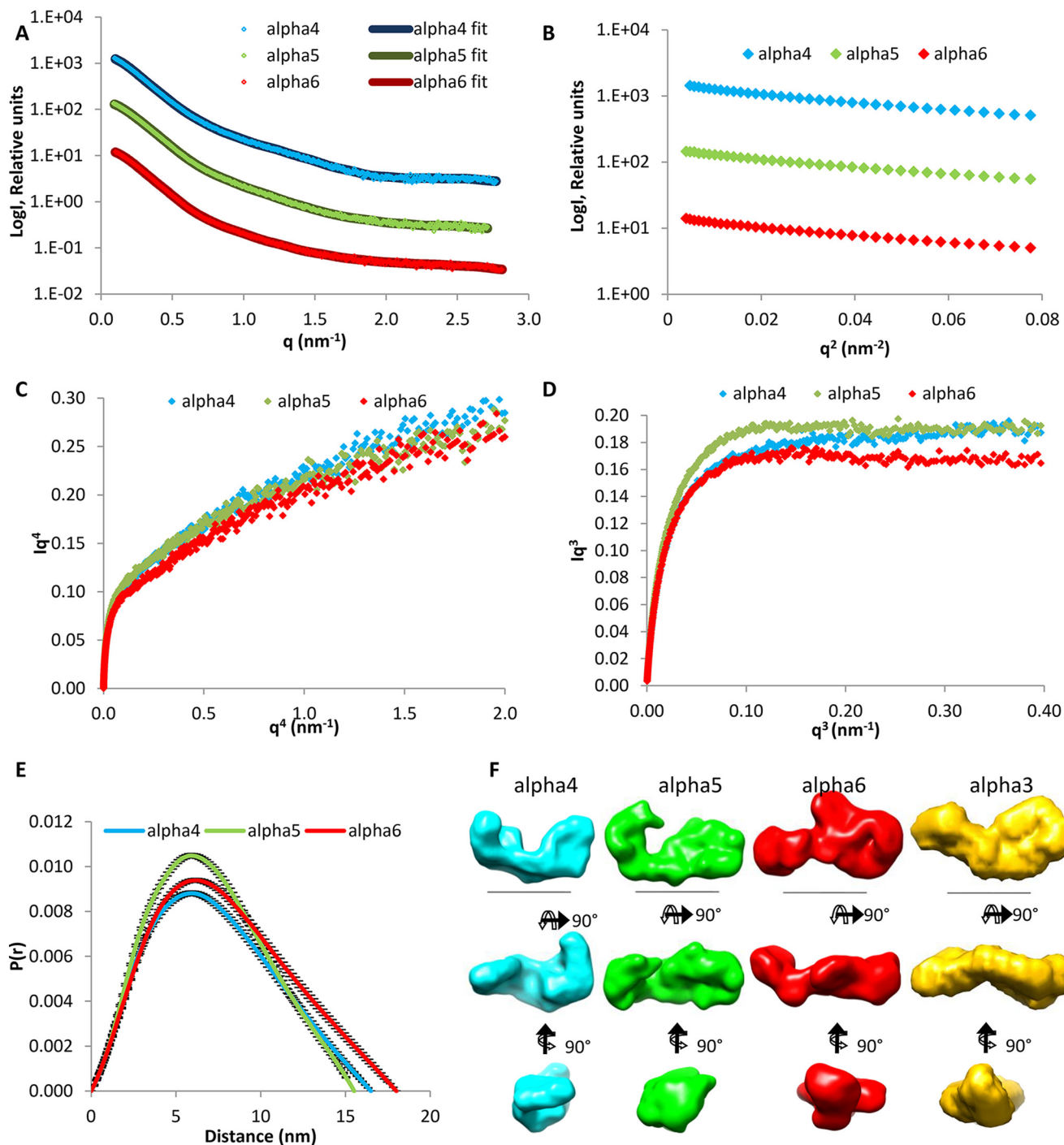
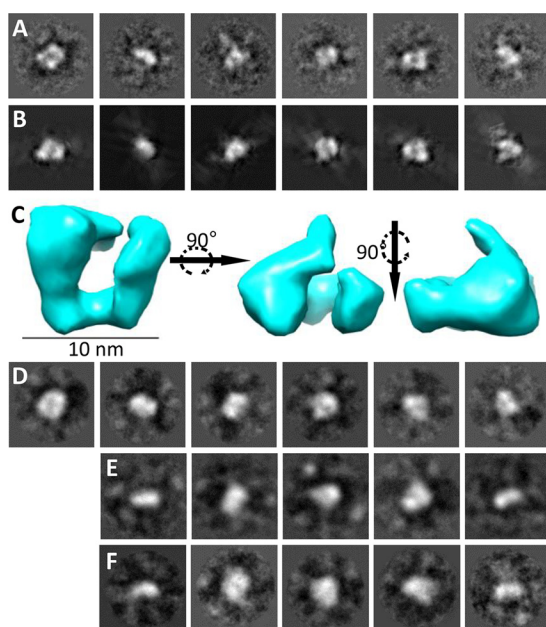


FIGURE 3. SAXS data collected for the N-terminal regions of the collagen VI  $\alpha 4$ ,  $\alpha 5$ , and  $\alpha 6$  chains. *A*, SAXS profile showing the log of x-ray scattering intensity ( $\text{Log}I$ ) as a function of the scattering vector  $q$  for the experimental scattering data with the DAMMIN fit with lowest  $\chi$  value superimposed. *B*, Guinier plot ( $\text{log}I$  versus  $q^2$ ) of the low  $q$  region of the x-ray scattering data where the radius of gyration ( $R_g$ ) can be measured from the gradient of the slope ( $-R_g^2/3$ ). *C*,  $q^4$  plot does not show a plateau, whereas the  $q^3$  plot (*D*) has a linear plateau that indicates some flexibility in the N-terminal regions. *E*,  $P(r)$  distribution plot shows the probability of different distances found within the protein. The longest distance is indicated by the  $D_{\text{max}}$ . *F*, *ab initio* models generated from the SAXS data shown in three orthogonal orientations. Scale bar, 10 nm. For all panels, the  $\alpha 4$ ,  $\alpha 5$ , and  $\alpha 6$  chains are shown in blue, green, and red, respectively. The *ab initio* model of the  $\alpha 3$  N9 to N1 region from Ref. 24 is shown in yellow for comparison.

bilon-P membranes (Millipore). The collagen VI chains were detected with affinity-purified antibodies raised against recombinant C-terminal regions. Secondary antibodies conjugated with horseradish peroxidase were used for detection by chemiluminescence (ECL). Collagen VI purified from whole newborn mouse carcasses and treated with 2 M urea was submitted to electropho-

resis on 0.5% agarose, 2.4% polyacrylamide composite gels under non-reducing conditions (34). IRDye700DX-conjugated sheep anti-rabbit IgG and IRDye800CW-conjugated goat anti-guinea pig IgG (Rockland) secondary antibodies were applied for multiplex detection, and bands were visualized using the Odyssey Infra-red Imaging System.



**FIGURE 4. Nanostructure of the N-terminal region of the collagen VI  $\alpha 4$  chain and comparison with the N-terminal regions of the  $\alpha 3$ ,  $\alpha 5$ , and  $\alpha 6$  chains.** *A*, representative class averages of the  $\alpha 4$  chain generated by reference-free classification using the IMAGIC-5 image processing and analysis software (Image Science, Germany). These class averages were used to generate the three-dimensional reconstruction. *B*, back-projections of the three-dimensional reconstruction, showing similarity to corresponding class averages. *C*, three-dimensional reconstruction of the N-terminal region of the  $\alpha 4$  chain generated by single particle analysis shown in three orthogonal views. *Scale bar*, 10 nm. Representative class averages generated by reference-free classification using the IMAGIC-5 software for the  $\alpha 3$  (*D*),  $\alpha 5$  (*E*), and  $\alpha 6$  chains (*F*). All boxes have a size of  $35.8 \times 35.8$  nm.

**SAXS Data Collection and Processing**—All protein samples were purified by size exclusion chromatography using a Superdex200 column on an ÄKTA Purifier FPLC in 10 mM phosphate buffer, 400 mM NaCl, pH 7.4, and concentrated using Vivaspin centrifugal concentrators if required. SAXS measurements of the N-terminal  $\alpha 4$ ,  $\alpha 5$ , and  $\alpha 6$  collagen VI chains ( $\sim 6$  mg/ml) with matched buffer blanks were collected on the I22 beamline at Diamond Light Source. The covered range of momentum transfer was  $0.014 < q < 0.48 \text{ \AA}^{-1}$  ( $q = 4 \pi \sin \theta / \lambda$ ) with detector distance of 2.5 m and x-ray wavelength of 0.1 nm. Data were collected in 120 successive 1-s frames to check for radiation damage. The data were normalized to the intensity of the incident beam and spherically averaged using an in-house program. Initial data processing and buffer subtraction were done in PRIMUS (35). SAXS measurements of the C-terminal collagen VI chains ( $\alpha 1$ , 4.3 mg/ml;  $\alpha 2$ , 4 mg/ml;  $\alpha 4$ , 3.5 mg/ml;  $\alpha 6$ , 3.5 mg/ml) with matched buffer blanks were collected at the EMBL-P12 beamline at PETRAIII (DESY, Hamburg, Germany) employing automated data acquisition and radial averaging protocols (36). For all data, the forward scattering intensity,  $R_g$ , and distance distribution function  $p(r)$  were evaluated with GNOM (37), and particle shapes were restored *ab initio* using DAMMIN (38).

Multiple runs were performed to generate 20 models that were combined and filtered to produce an averaged model using the DAMAVER (39) software package.  $\chi$  fitting values and the normalized spatial discrepancy for *ab initio* modeling is shown in Table 2. Rigid body modeling against the

experimental SAXS data was performed with SASREF (40) using individual VWA domains with a distance range of 10–15 Å between each domain. Because the N-terminal regions were flexible, they were analyzed as an ensemble; 10,000 models were generated using RANCH, and an ensemble of models representing the experimental SAXS data were generated by EOM (41).

**Electron Microscopy and Single-particle Analysis**—Collagen VI  $\alpha 4$ ,  $\alpha 5$ , and  $\alpha 6$  N-terminal regions ( $\sim 50 \mu\text{g/ml}$ ) were adsorbed onto glow-discharged carbon-coated grids and stained with 4% (w/v) uranyl acetate, pH 4.7. Grids were observed using an FEI Tecnai Twin (120 keV) transmission EM, and images were recorded under low dose conditions ( $< 10 \text{ e}^-/\text{\AA}^2$ ) on  $2048 \times 2048$  pixel CCD camera at  $\times 30,000$  (2.8 Å/pixel) between  $-0.2$ - and  $-2.0$ - $\mu\text{m}$  defocus. Imagic-5 (42) was used for particle picking and image processing. Images were contrast transfer function corrected, and the total numbers of particles in each dataset were 6047 for  $\alpha 4$ ; 5552 for  $\alpha 3$ ; 2745 for  $\alpha 5$ , and 2129 for  $\alpha 6$ . Characteristic class-sum images were used as references to align the dataset. For the  $\alpha 4$  chain, angular reconstitution produced unique projection classes, enabling calculation of an initial three-dimensional reconstruction that was then subjected to five rounds of iterative refinement. The resolution was estimated by Fourier shell correlation as  $\sim 40$  Å using the 0.5 correlation criteria.

**Immunolectron Microscopy on Natively Extracted Microfibrils**—Native collagen VI microfibrils were extracted from E14.5 mouse lungs by collagenase digestion in analogy to previously described protocols for bovine cornea (43) with modifications as described in Ref. 44. The distribution of the different  $\alpha$  chains in collagen VI preparations was analyzed by incubation for 30 min at 37 °C with colloidal gold-labeled (45) antibodies specific for the N-terminal regions of the long collagen VI  $\alpha$  chains (13) followed by negative staining and transmission electron microscopy as described (46). Specimens were observed in a Philips/FEI CM 100 TWIN transmission electron microscope (FEI Co.) at 60-kV accelerating voltage. Images were recorded with a side-mounted Olympus Veleta camera with a resolution of  $2048 \times 2048$  pixels using ITEM<sup>TM</sup> software. All electron microscopic work was performed at the Core Facility for Integrated Microscopy, Panum Institute, University of Copenhagen.

## Results

**Recombinant Expression of N- and C-terminal Globular Regions of Collagen VI**—The globular non-collagenous regions of the different collagen VI  $\alpha$  chains are important for assembly and structure of the complex microfibrillar network that is present in nearly all tissues. Therefore, N- and C-terminal globular regions of the  $\alpha 1$ – $\alpha 6$  chains of collagen VI were recombinantly expressed in the eukaryotic HEK293-EBNA cells and used for structural analysis. The proteins were tagged with the One-STrEP-tag and affinity-purified. SDS-PAGE often revealed a heterogeneous band pattern, both under reducing and non-reducing conditions due to proteolytic processing and the formation of disulfide-linked oligomers (data not shown). For some experiments, the proteins were therefore further

## Heterogeneity of Collagen VI Microfibrils

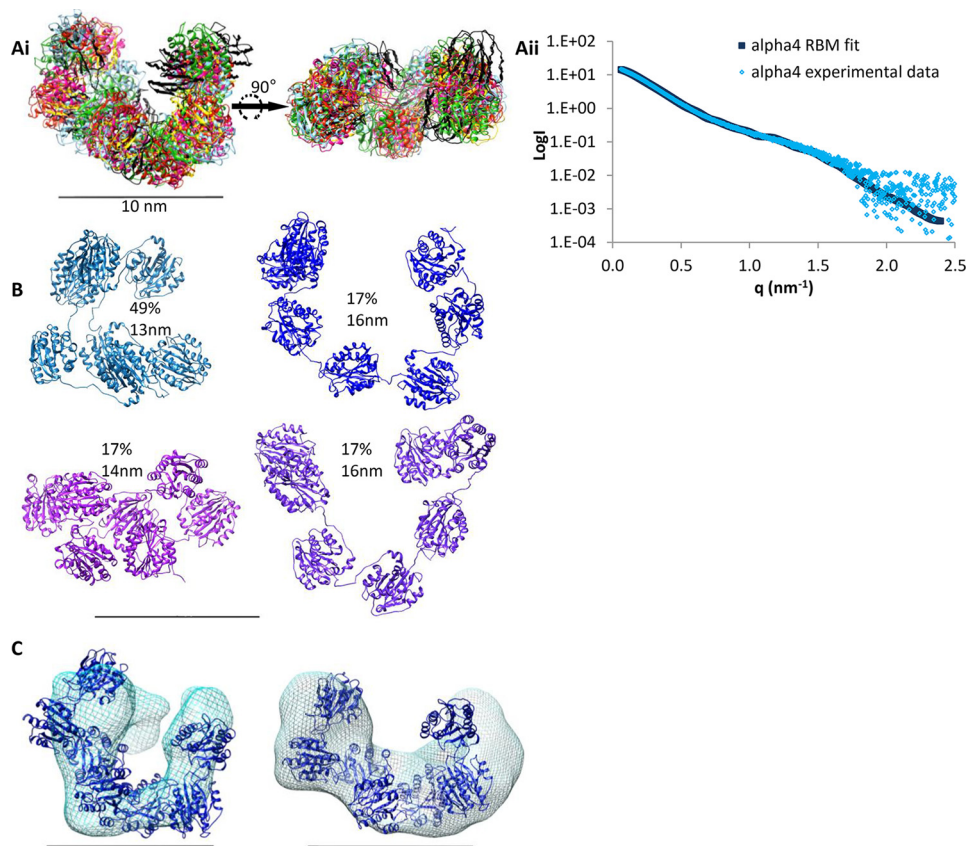


FIGURE 5. **Rigid body modeling of the N-terminal region of the collagen VI  $\alpha 4$  chain and comparison with SAXS *ab initio* and EM data.** *A, panel i*, six superimposed RBM simulations for the N-terminal region of the  $\alpha 4$  chain shown in two orientations and the theoretical scattering of the rigid body modeling with lowest  $\chi$  value compared with the experimental scattering data (*A, panel ii*). *B*, ensemble of models produced using EOM from the x-ray scattering data and their relative proportions and maximum dimension ( $D_{\max}$ ). *C*, EM map (*left*) and *ab initio* model (*right*) for the N-terminal region of the  $\alpha 4$  chain both with a representative model superimposed. For all panels the scale bar is 10 nm.

purified by size-exclusion chromatography (Fig. 2). Some of the recombinant proteins ( $\alpha 3C$ – $\alpha 6C$ ) were used for immunization of rabbits and guinea pigs to generate antisera specific for the respective globular regions.

***Ab Initio SAXS Models of the N-terminal Globular Regions of the  $\alpha 4$ ,  $\alpha 5$ , and  $\alpha 6$  Chains Indicate a C-shaped Structure***—The first step was to determine the structure of the large N-terminal regions of the novel  $\alpha 4$ ,  $\alpha 5$ , and  $\alpha 6$  chains that resemble the  $\alpha 3$  chain by sequence and domain structure and are thought to replace the  $\alpha 3$  chain in some collagen VI molecules (11). It was therefore relevant to determine the shape of the N-terminal globular regions for these chains that could then be compared with a SAXS model of the large N-terminal globular region of the collagen VI  $\alpha 3$  chain. It has been shown that this region has a compact C-shaped structure that is likely to participate in the assembly of collagen VI (24). SAXS measurements were performed at the Diamond Light Source, beamline I22. Size-exclusion chromatography was carried out upstream of the beamline and the monomer fractions used (Fig. 3A). Guinier plots of the x-ray scattering results allowed assessment of data quality (Fig. 3B). In contrast to the  $q^4$  plot (Fig. 3C), the  $q^3$  plot (Fig. 3D) showed a linear plateau that indicates some flexibility in the N-terminal regions (47). Distance distribution plots revealed longest distances of 15.6, 16.5, and 18.0 nm for the  $\alpha 5$ ,  $\alpha 4$ , and  $\alpha 6$  chains, respectively (Fig. 3E), and *ab initio* models were generated (Fig. 3F) with DAMMIN (38). All three models display a

C-shaped conformation reminiscent of that of the  $\alpha 3$  chain N-terminal globular region (Fig. 3F) (24).

***Single Particle EM Nanostructure of the N-terminal Globular Region of the  $\alpha 4$  Chain Confirms the C-shaped Structure Revealed by SAXS***—To confirm the SAXS models, single particle EM was performed after negative staining with uranyl acetate. The N-terminal globular region of the  $\alpha 4$  chain was chosen as a prototype. 6047 single molecules were selected with the Imagic-5 program (42), and reference-free class averages were generated (Fig. 4A) and used for the calculation of a three-dimensional model (Fig. 4C). A structure similar to the C-shaped SAXS model was obtained (Fig. 3F). The quality of the model was tested by back-projections showing similarity to the corresponding class averages (Fig. 4B). Single particle EM was also performed on the N-terminal globular regions of the  $\alpha 3$ ,  $\alpha 5$ , and  $\alpha 6$  chains (Fig. 4, D–F). The general appearance of the class averages was similar, but the numbers of examined single molecules and orientations observed were not sufficient to obtain a three-dimensional structure. Recently, the crystal structure of a single collagen VI VWA domain ( $\alpha 3N5$ ) was determined (26). This structure was used for rigid body modeling of the  $\alpha 4$  chain N terminus to model domain organization from the SAXS data. The program SASREF (40) was used and generated six models that were similar and could be superimposed to show a C-shaped structure (Fig. 5A). As the  $q^4$  plot suggested flexibility in the N-terminal regions (Fig. 3C), ensemble analysis was also

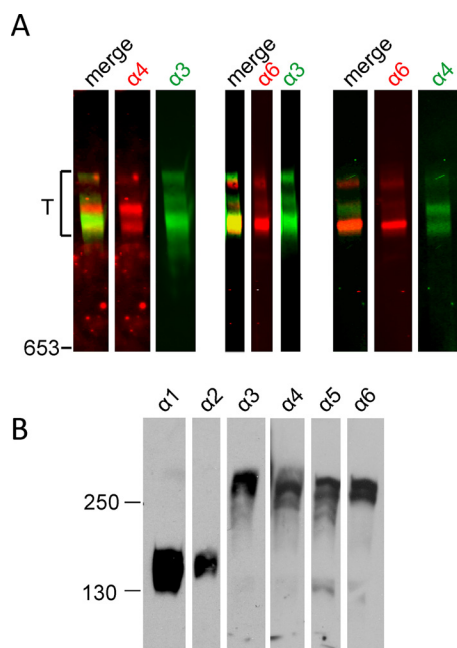


**FIGURE 6. Immunoblot analysis of collagen VI.** *A*, collagen VI purified from whole newborn mouse carcasses was separated in agarose/polyacrylamide composite gels under non-reducing conditions and was detected with affinity-purified chain-specific long chain antibodies from rabbit ( $\alpha 4$  and  $\alpha 6$ , red) and guinea pig ( $\alpha 3$  and  $\alpha 4$ , green) and secondary antibodies labeled with spectrally distinct infrared fluorescent dyes. The relative mobility of tetramers is indicated (*T*). *B*, collagen VI purified from whole newborn mouse carcasses was separated in normal SDS-polyacrylamide gels under reducing conditions and detected with polyclonal antibodies specific for the collagen VI  $\alpha 1$ – $\alpha 6$  chains.

used to model different conformers. 10,000 models were generated of the  $\alpha 4$  chain N terminus and compared with the experimental scattering data using EOM (41). An ensemble of four models was predicted with an average  $D_{\max}$  of 14.8 nm (Fig. 5*B*). The ensemble included two models that contributed 34% of the ensemble with an open C-shape ( $D_{\max} = 16.4$  nm), and one model contributing 49% of the ensemble had a more compact C-shape ( $D_{\max} = 13.3$  nm). The more open shapes have a similar  $D_{\max}$  to that predicted from the experimental data (16.5 nm). Comparing the *ab initio* SAXS model and the EM-based model revealed the strongest agreement with the rigid body model that had an intermediate conformation between the open and closed C-shape. The convergence of different low resolution structural data on a C-shaped model reflects the reliability of this conformation of the N-terminal globular region of the  $\alpha 4$  chain (Fig. 5*C*).

*Collagen VI Extracted from Tissue Contains Novel Long Chains Incorporated into Mixed Microfibrils*—Because we showed that the N-terminal regions of the novel long collagen VI chains,  $\alpha 4$ ,  $\alpha 5$ , and  $\alpha 6$ , have a similar structure as the  $\alpha 3$  chain, the next question was whether they form tetramers and microfibrils similar to those that contain the  $\alpha 3$  chain? So far, their assembly into higher order structures has been only sparsely studied. However, the novel long chains are lacking in the extracellular matrix of Col6a1<sup>-/-</sup> mice, indicating that they are contained in or associated with the classical collagen VI microfibrils (13). Three important questions remain. 1) Do the novel long collagen VI chains also assemble into tetramers, as has been shown for collagen VI molecules containing the  $\alpha 3$

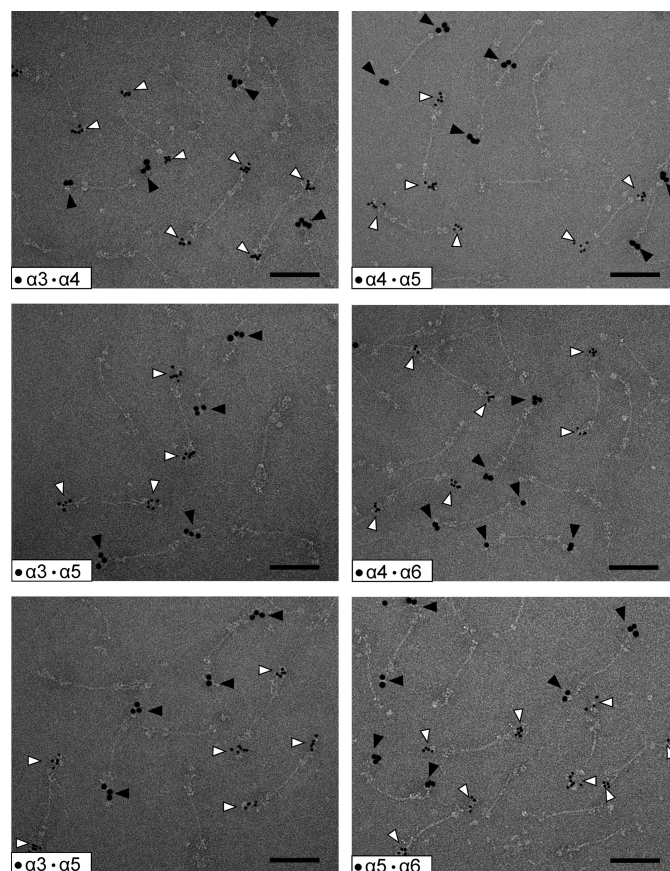


**FIGURE 7. Composition of collagen VI tetramers as detected by electron microscopy after negative staining.** Representative collagen VI tetramers from E14.5 mouse lung containing different long  $\alpha$  chains are shown. Only homotetramers were detected. The N-terminal regions of the long chains were doubly labeled using specific gold-labeled antibodies against the different  $\alpha$  chains. Small gold particles (open arrowheads) always stain the  $\alpha$  chain with the lower number, whereas the large gold particles (filled arrowheads) stain that with the higher number. Scale bar, 100 nm.

chain? 2) If so, what is the composition of the tetramers, are they homotetramers<sup>5</sup> or heterotetramers with regard to long chain composition? 3) Do collagen VI molecules containing the novel long chains assemble into microfibrils at all and, if so, what is the composition of these? To answer these questions, we studied collagen VI extracted from tissue. First, we used collagen VI purified from whole newborn mouse carcasses. By electrophoresis on composite SDS agarose/polyacrylamide gels we could show that collagen VI oligomers containing the  $\alpha 4$  or  $\alpha 6$  chains migrate to positions that are similar to those of tetramers containing the  $\alpha 3$  chain (Fig. 6*A*). By multiplex detection, using affinity-purified chain-specific long chain antibodies from rabbit and guinea pig and secondary antibodies labeled with spectrally distinct infrared fluorescent dyes, we could detect bands that migrate to both similar and different positions. The bands that migrate at similar positions could either be heterotetramers or homo-oligomers that coincidentally co-migrate due to similar size. However, there are bands that migrate at positions where mostly no other bands appear, *e.g.*

<sup>5</sup> Homotetramers are tetramers of monomeric heterotrimeric collagen VI molecules composed of one  $\alpha 1$  chain, one  $\alpha 2$  chain, and one of the alternative  $\alpha 3$ ,  $\alpha 4$ ,  $\alpha 5$ , or  $\alpha 6$  chains see Fig. 11.

## Heterogeneity of Collagen VI Microfibrils

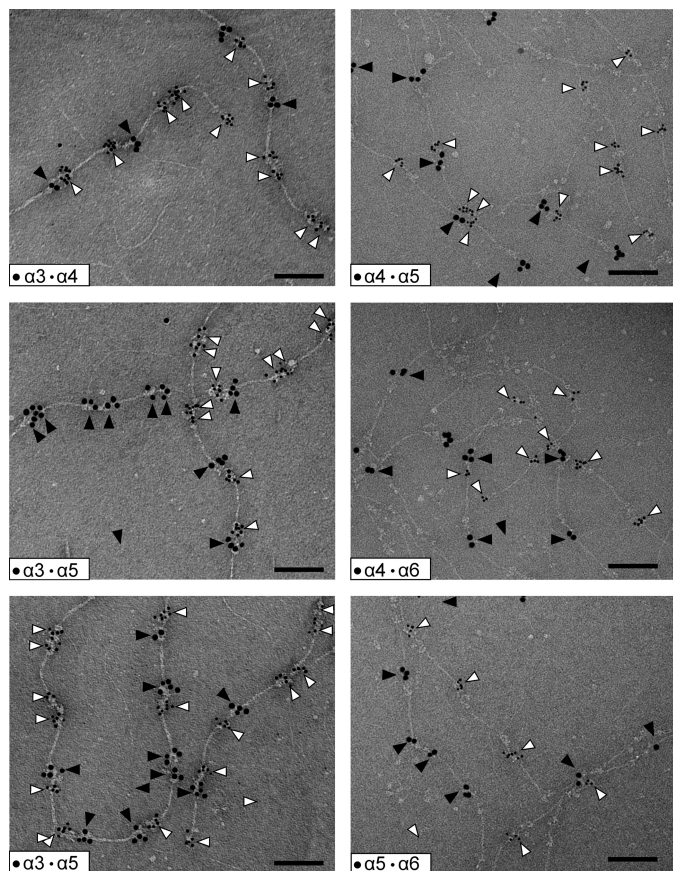


**FIGURE 8. Structure of collagen VI microfibrils as detected by electron microscopy after negative staining.** Representative collagen VI microfibrils from E14.5 mouse lung composed of tetramers containing different long chains are shown. Only homotetramers were detected. The N-terminal regions of the long chains were double labeled using specific gold-labeled antibodies against the different  $\alpha$  chains. Small gold particles (*open arrowheads*) always stain the  $\alpha$  chain with the lower number, whereas the large gold particles (*filled arrowheads*) stain that with the higher number. Note that as the tetramers overlap the “outer” globules belong to the same tetramer, and the “inner” globules belong to the neighboring tetramers. This is indicated in Fig. 11 in a schematic drawing of the mixed  $\alpha 3/\alpha 6$  microfibril. Scale bar, 100 nm.

the major  $\alpha 4$  chain band. This clearly indicates that at least a portion of the long chains form homo-oligomers. The  $\alpha 5$  chain could only be detected by SDS-PAGE under reducing conditions (Fig. 6B), and for this chain it was therefore not possible to determine whether it forms homo-oligomers or heterotetramers. Neither could the composition of the co-migrating  $\alpha 4$  or  $\alpha 6$  chain tetramers be determined. Only a method where individual microfibrils can be studied by use of chain-specific antibodies is suitable to address this question. Consequently, immunoelectron microscopy was performed on natively extracted collagen VI from E14.5 mouse lung where all four long chains are expressed. Interestingly, we could only detect homotetramers, irrespective of whether single tetramers (Fig. 7) or microfibrils were labeled (Fig. 8). In microfibrils, the “outer” globules representing the N-terminal globules were always labeled with the same antibody. As the assembled tetramers overlap, these belong to the same tetramer, in contrast to the “inner” globules that belong to the neighboring tetramers. Tetramers stained with two different antibodies were not observed. Strikingly, in all double labelings using all combinations of antibodies, we

could identify mixed microfibrils composed of homotetramers containing different long  $\alpha$  chains throughout.

*Models of the C-terminal Globular Regions of the  $\alpha 1$ ,  $\alpha 2$ ,  $\alpha 4$ , and  $\alpha 6$  Chains Give Insight into Their Role during Assembly*—Having shown that the shapes of the N-terminal domains of long collagen VI  $\alpha$  chains are similar and that these chains therefore have the potential to replace each other in assembly, we wanted to provide structural information on the C-terminal regions of the different  $\alpha$  chains, as at least in the  $\alpha 1$  and  $\alpha 2$  chains these regions appear to be involved in collagen VI assembly (48). So far, except for the Kunitz domain (25) of the  $\alpha 3$  chain, there is no structural information on the C-terminal globular regions of the collagen VI chains beyond single EM images. We therefore performed SAXS measurements on the C-terminal fragments of the  $\alpha 1$ ,  $\alpha 2$ ,  $\alpha 4$ , and  $\alpha 6$  chains at PetraIII (beamline P12) (Fig. 9A). The C-terminal fragments of the  $\alpha 3$  and the  $\alpha 5$  chains could not be purified at the concentrations that are required for SAXS measurements. Guinier plots of the x-ray scattering data allowed assessment of data quality (Fig. 9B). The  $q^4$  plots showed a linear region indicating little flexibility in the C-terminal regions (Fig. 9C). Distance distribution plots revealed longest distances of 12.5, 14.1, 20.5, and 13.4 nm for the  $\alpha 1C$ ,  $\alpha 6C$ ,  $\alpha 4C$ , and  $\alpha 2C$  chains, respectively (Fig. 9D). Interestingly, the molecular weight of the C-terminal globular regions of the  $\alpha 1$ ,  $\alpha 2$ , and  $\alpha 4$  chains is consistent with dimers from the volume of correlation (49), and these were processed with P2 symmetry. *Ab initio* modeling revealed elongated structures for each  $\alpha$  chain (Fig. 9E). Because  $\alpha 1C$  and  $\alpha 2C$ , like the N-terminal globular regions, consist only of VWA domains, rigid body modeling using the structural data from the N5 domain of the  $\alpha 3$  chain was performed (Fig. 10A). The models fit well into the *ab initio* SAXS model, and the  $\alpha 1C$  and  $\alpha 2C$  structures are very similar. In each case, dimerization occurs via a contact between one of the tandem VWA domains leading to a staggered “zigzag” conformation (Fig. 10, B and C).  $\alpha 4C$  and  $\alpha 6C$  contain other domains without known structure in addition to VWA domains, and therefore rigid body modeling could not be performed. However, four VWA domains can be accommodated in the central density of the *ab initio* model of  $\alpha 4C$ , and one pair of VWA domains in the *ab initio* model of  $\alpha 6C$  where the additional unique domain is seen as an elongated protrusion (Fig. 10, D and E).

## Discussion

The formation of collagen VI microfibrils is a complex multistep process. Already in the secretory pathway 12  $\alpha$  chains assemble to tetramers that have a molecular mass similar to that of ribosomes. After secretion, these tetramers assemble to form an extended microfibrillar network. The presence of alternative long  $\alpha$  chains that may replace the  $\alpha 3$  chain adds to the complexity of collagen VI assemblies. The lack of structural information hinders the in-depth understanding of the assembly process and of the impact of mutations that lead to muscular dystrophies.

The lack of expression of the novel long collagen VI chains in collagen VI  $\alpha 1$  chain-deficient mice was a first indication for their participation in the assembly of collagen VI molecules (11). Further evidence supporting that the novel long chains

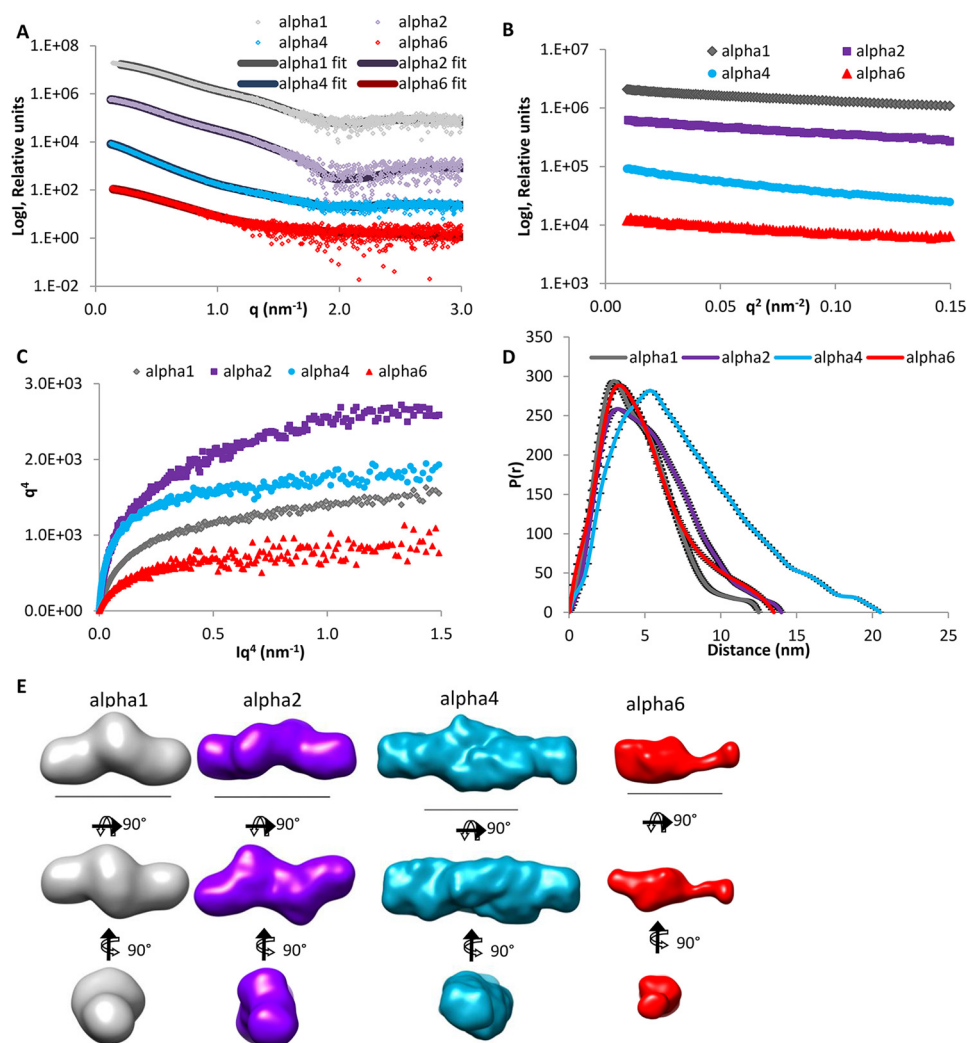


FIGURE 9. **SAXS data collected for the C-terminal regions of the collagen VI  $\alpha 1$ ,  $\alpha 2$ ,  $\alpha 4$ , and  $\alpha 6$  chains.** *A*, SAXS profile showing the log of x-ray scattering intensity ( $\text{Log}I$ ) as a function of the scattering vector  $q$  for the experimental scattering data with the DAMMIN fit with lowest  $\chi$  value superimposed. *B*, Guinier plot ( $\text{log}I$  versus  $q^2$ ) of the low  $q$  region of the x-ray scattering data where the radius of gyration ( $R_g$ ) can be measured from the gradient of the slope ( $-R_g^2/3$ ). *C*,  $q^4$  plot has a linear plateau that indicates that these regions are not flexible. *D*,  $P(r)$  distribution plot shows the probability of different distances found within the protein. The longest distance is indicated by the  $D_{\text{max}}$ . *E*, *ab initio* models generated from the SAXS data shown in three orthogonal orientations. Scale bar, 10 nm. For all panels, the  $\alpha 1$ ,  $\alpha 2$ ,  $\alpha 4$ , and  $\alpha 6$  chains are shown in gray, purple, blue, and red, respectively.

may replace the  $\alpha 3$  chain in assembly came from SAXS measurements and single molecule EM of their large N-terminal globular regions. The SAXS models of the novel long chains show monomeric structures that have a similar shape as that of the  $\alpha 3$  chain N-terminal region. The SAXS results were confirmed by single particle EM of the N-terminal globular region of the  $\alpha 4$  chain. The determined nanostructure as well as the *ab initio* SAXS model and the rigid body model all resemble the compact C-shape found for this region of the  $\alpha 3$  chain. The consistently monomeric state indicates that self-interactions between the N-terminal regions are not involved at any stage of assembly.

Because of the striking similarity of the shape of the long chain N-terminal regions, we further investigated how these are integrated into microfibrils. Collagen VI purified from newborn mouse carcasses was studied by immunoblot analysis after composite SDS-agarose/PAGE. Under non-reducing conditions, collagen VI oligomers containing the  $\alpha 4$  and  $\alpha 6$  chains migrated close to oligomers containing the  $\alpha 3$  chain, indicating

that the novel long chains also assemble into homotetramers. However, as some bands co-migrate it could not be determined whether these are homotetramers containing only one long chain or heterotetramers. Interestingly, the  $\alpha 5$  chain was detected only under reducing conditions, indicating that this  $\alpha 5$  chain is disulfide-linked to other polypeptides or that  $\alpha 5$  chain-containing tetramers are scarce and below the detection limit. However, antibody labeling followed by electron microscopy more clearly revealed how collagen VI containing the novel long chains assembles. When microfibrils from E14.5 mouse lung were labeled with affinity-purified, gold-labeled antibodies against the long chains, all four were shown to be part of collagen VI microfibrils with the typical beads-on-a-string appearance. These experiments unequivocally demonstrated that the assembly of collagen VI molecules containing the novel long chains must be very similar to those containing the  $\alpha 3$  chain. Moreover, we could only detect homotetramers containing only one of the long chains  $\alpha 3$ ,  $\alpha 4$ ,  $\alpha 5$ , or  $\alpha 6$  when studying individual tetramers or homotetramers as building

## Heterogeneity of Collagen VI Microfibrils

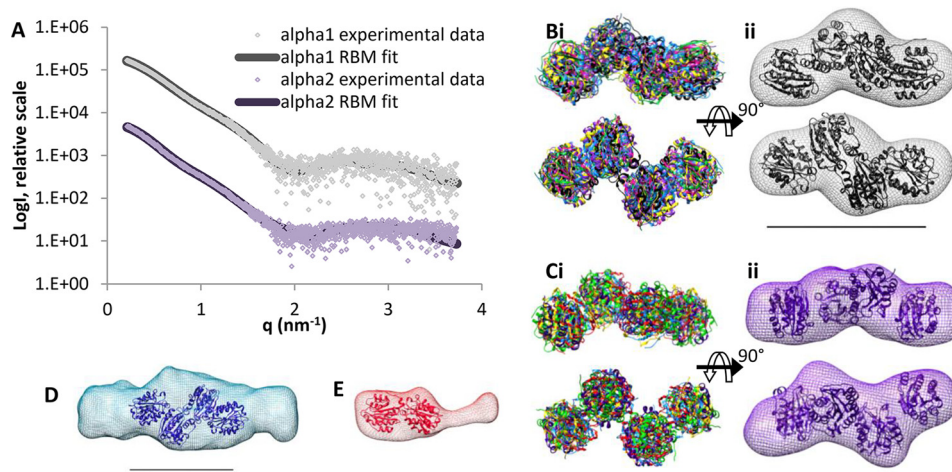


FIGURE 10. **Rigid body modeling of collagen VI C-terminal regions and comparison with SAXS *ab initio* models.** *A*, theoretical scattering of representative RBMs was compared with the experimental scattering data of the C-terminal regions of the  $\alpha 1$  and  $\alpha 2$  chains. *B*, *panel i*, six superimposed RBM simulations for the C-terminal region of the  $\alpha 1$  chain, and *panel ii*, *ab initio* model for the C-terminal region of the  $\alpha 1$  chain with a representative RBM superimposed, both shown in two orientations. *C*, similar to the C-terminal region of the  $\alpha 2$  chain. *D*, two VWA domain pairs superimposed into the  $\alpha 4$  chain *ab initio* model indicating that the C-terminal region of the  $\alpha 4$  chain is dimeric with four VWA domains accommodated in the central density and two symmetric protrusions. *E*, however, the C-terminal region of the  $\alpha 6$  chain is monomeric and can only accommodate one VWA domain pair and the additional domain is seen as an elongated protrusion. For all panels the scale bar is 10 nm.

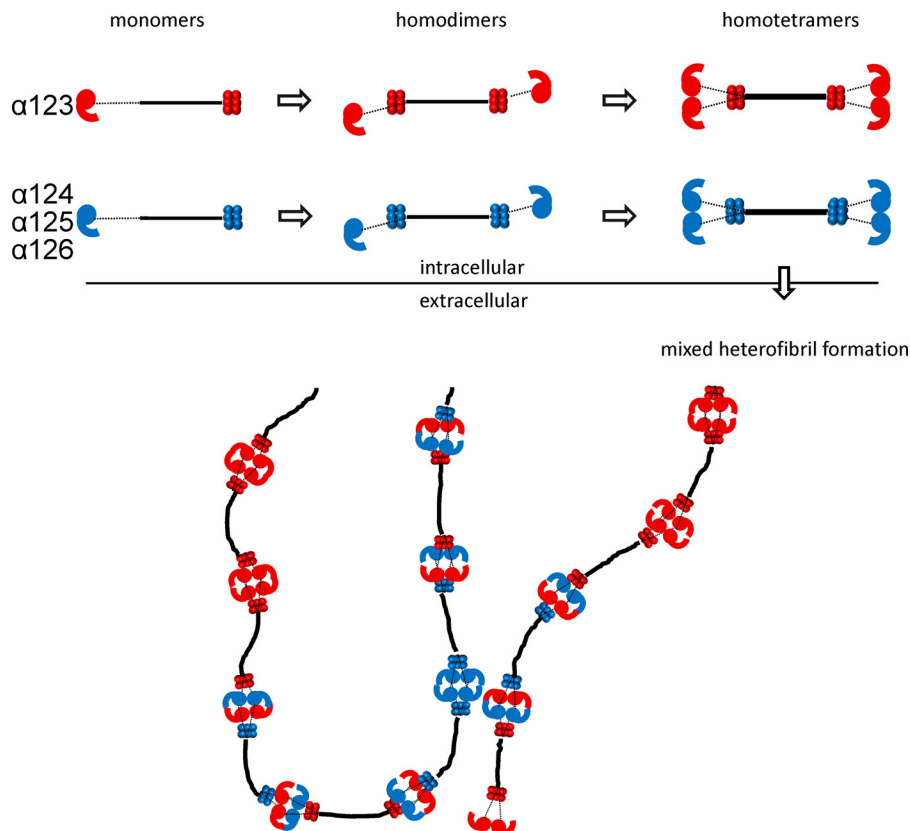


FIGURE 11. **Assembly of heterogeneous collagen VI microfibrils.** Schematic drawing of the assembly of the heterogeneous microfibrils. The composition of the schematically drawn microfibrils below reflects the composition of the mixed microfibrils containing the  $\alpha 3$  and the  $\alpha 6$  chain shown in Fig. 8. Collagenous domain, *black*; non-collagenous regions of the  $\alpha 3$  chain, *red*; non-collagenous regions of the  $\alpha 4$ ,  $\alpha 5$ , and  $\alpha 6$  chains, *blue*.

units in microfibrils. In the microfibrils, homotetramers that contain either the same or a different long chain assemble end to end but with an overlap. The formation of mixed microfibrils of differing composition (schematically shown in Fig. 11) adds another level of complexity to the assembly of collagen VI. As the novel long chains have a restricted tissue distribution, it is

likely that the mixed fibrils have specific functions in regions where a particular novel chain is expressed. One such function could be their integration into the extracellular matrix. As it was suggested that the N-terminal globule of the  $\alpha 3$  chain projects out from the rest of the molecule, potentially providing interaction surfaces for other cell surface or matrix molecules

(24), the different long chains could interact with alternative molecules. Indeed, by electron microscopy of skeletal muscle using gold labeled antibodies, it was shown that the  $\alpha 6$  chain is restricted to the reticular lamina of muscle fibers but is absent at both the interface with the lamina densa and the basement membrane of capillaries (13). In contrast, the  $\alpha 3$  chain is present at all these sites. The novel long chains may also alter the mechanical properties of the microfibrils, particularly as they contain significantly more cysteine residues than the  $\alpha 3$  chain (Fig. 1). These could alter the microfibril flexibility by formation of additional disulfide bonds.

In contrast to the large N-terminal globular regions, SAXS models of some C-terminal globular regions indicated their involvement in assembly, as the C-terminal globular regions of the collagen VI  $\alpha 1$ ,  $\alpha 2$ , and  $\alpha 4$  chains, but not that of the  $\alpha 6$  chain, appeared as dimers. Indeed, according to the most recent assembly model (Beecher *et al.* (24)), tetramer formation, but not dimer formation, may require a contact between  $\alpha 1$  and  $\alpha 2$  chains, and therefore self-interactions could play a role in tetramer formation. This is supported by the presence of dimers but the absence of tetramers in a patient with autosomal recessive myosclerosis myopathy lacking the C2 domain of the  $\alpha 2$  chain (17). Moreover, *in vitro* transfection experiments indicated a role for the C2 domains of the  $\alpha 1$  and  $\alpha 2$  chains in collagen VI assembly (48).

The analysis of the structure of the non-collagenous regions of collagen VI gave further insight into their role during assembly and for the composition of microfibrils. The presence of three novel long chains adds to the complexity of collagen VI microfibrillar assemblies. Further experiments are needed to analyze differences between collagen VI microfibrils of different composition, *e.g.* their integration into the extracellular matrix, their exact localization, and their contribution to the mechanical properties of the tissue.

**Author Contributions**—C. B., M. P., and R. W. conceived and designed the experiments. C. B., C. P. B., M. M., S. L., and T. M. performed the experiments. C. B., C. P. B., M. M., M. P., R. W., and T. M. analyzed the data. P. B. contributed essential materials. C. B., M. P., and R. W. contributed to the writing of the manuscript. All authors reviewed the results and approved the final version of the manuscript.

**Acknowledgments**—We are grateful to the staff in the EM facility at the Faculty of Life Sciences, University of Manchester, and the Core Facility for Integrated Microscopy, Panum Institute, University of Copenhagen, for providing a cutting edge environment for electron microscopy. We thank Maria Baumgarten for skillful work. We also thank Petra III and Diamond Light Source for SAXS beamtime on beamlines P12 and I22, respectively, and Drs. Cy Jeffries and Katsuaki Inoue for assistance during data collection.

## References

- Cescon, M., Gattazzo, F., Chen, P., and Bonaldo, P. (2015) Collagen VI at a glance. *J. Cell Sci.* **128**, 3525–3531
- Keene, D. R., Engvall, E., and Glanville, R. W. (1988) Ultrastructure of type VI collagen in human skin and cartilage suggests an anchoring function for this filamentous network. *J. Cell Biol.* **107**, 1995–2006
- Bidanset, D. J., Guidry, C., Rosenberg, L. C., Choi, H. U., Timpl, R., and Hook, M. (1992) Binding of the proteoglycan decorin to collagen type VI. *J. Biol. Chem.* **267**, 5250–5256
- Burg, M. A., Tillet, E., Timpl, R., and Stallcup, W. B. (1996) Binding of the NG2 proteoglycan to type VI collagen and other extracellular matrix molecules. *J. Biol. Chem.* **271**, 26110–26116
- Finnis, M. L., and Gibson, M. A. (1997) Microfibril-associated glycoprotein-1 (MAGP-1) binds to the pepsin-resistant domain of the  $\alpha 3$ (VI) chain of type VI collagen. *J. Biol. Chem.* **272**, 22817–22823
- Wiberg, C., Klatt, A. R., Wagener, R., Paulsson, M., Bateman, J. F., Heinegård, D., and Mörgelin, M. (2003) Complexes of matrilin-1 and biglycan or decorin connect collagen VI microfibrils to both collagen II and aggrecan. *J. Biol. Chem.* **278**, 37698–37704
- Chu, M. L., Pan, T. C., Conway, D., Saitta, B., Stokes, D., Kuo, H. J., Glanville, R. W., Timpl, R., Mann, K., and Deutzmann, R. (1990) The structure of type VI collagen. *Ann. N.Y. Acad. Sci.* **580**, 55–63
- Furthmayr, H., Wiedemann, H., Timpl, R., Odermatt, E., and Engel, J. (1983) Electron-microscopical approach to a structural model of intima collagen. *Biochem. J.* **211**, 303–311
- Engvall, E., Hesse, H., and Klier, G. (1986) Molecular assembly, secretion, and matrix deposition of type VI collagen. *J. Cell Biol.* **102**, 703–710
- Fitzgerald, J., Rich, C., Zhou, F. H., and Hansen, U. (2008) Three novel collagen VI chains,  $\alpha 4$ (VI),  $\alpha 5$ (VI), and  $\alpha 6$ (VI). *J. Biol. Chem.* **283**, 20170–20180
- Gara, S. K., Grumati, P., Urciuolo, A., Bonaldo, P., Kobbe, B., Koch, M., Paulsson, M., and Wagener, R. (2008) Three novel collagen VI chains with high homology to the  $\alpha 3$  chain. *J. Biol. Chem.* **283**, 10658–10670
- Wagener, R., Gara, S. K., Kobbe, B., Paulsson, M., and Zaucke, F. (2009) The knee osteoarthritis susceptibility locus DVWA on chromosome 3p24.3 is the 5' part of the split COL6A4 gene. *Matrix Biol.* **28**, 307–310
- Gara, S. K., Grumati, P., Squarzoni, S., Sabatelli, P., Urciuolo, A., Bonaldo, P., Paulsson, M., and Wagener, R. (2011) Differential and restricted expression of novel collagen VI chains in mouse. *Matrix Biol.* **30**, 248–257
- Bushby, K. M., Collins, J., and Hicks, D. (2014) Collagen type VI myopathies. *Adv. Exp. Med. Biol.* **802**, 185–199
- Bönnemann, C. G. (2011) The collagen VI-related myopathies Ullrich congenital muscular dystrophy and Bethlem myopathy. *Handb. Clin. Neurol.* **101**, 81–96
- Scacheri, P. C., Gillanders, E. M., Subramony, S. H., Vedanarayanan, V., Crowe, C. A., Thakore, N., Bingler, M., and Hoffman, E. P. (2002) Novel mutations in collagen VI genes: expansion of the Bethlem myopathy phenotype. *Neurology* **58**, 593–602
- Merlini, L., Martoni, E., Grumati, P., Sabatelli, P., Squarzoni, S., Urciuolo, A., Ferlini, A., Gualandri, F., and Bonaldo, P. (2008) Autosomal recessive myosclerosis myopathy is a collagen VI disorder. *Neurology* **71**, 1245–1253
- Zech, M., Lam, D. D., Francescato, L., Schormair, B., Salminen, A. V., Jochim, A., Wieland, T., Lichtner, P., Peters, A., Gieger, C., Lochmüller, H., Strom, T. M., Haslinger, B., Katsanis, N., and Winkelmann, J. (2015) Recessive mutations in the  $\alpha 3$  (VI) collagen gene COL6A3 cause early-onset isolated dystonia. *Am. J. Hum. Genet.* **96**, 883–893
- Hunter, J. M., Ahearn, M. E., Balak, C. D., Liang, W. S., Kurdoglu, A., Corneveaux, J. J., Russell, M., Huentelman, M. J., Craig, D. W., Carpten, J., Coons, S. W., DeMello, D. E., Hall, J. G., Bernes, S. M., and Baumbach-Reardon, L. (2015) Novel pathogenic variants and genes for myopathies identified by whole exome sequencing. *Mol. Genet. Genomic Med.* **3**, 283–301
- Bonaldo, P., Braghetta, P., Zanetti, M., Piccolo, S., Volpin, D., and Bressan, G. M. (1998) Collagen VI deficiency induces early onset myopathy in the mouse: an animal model for Bethlem myopathy. *Hum. Mol. Genet.* **7**, 2135–2140
- Irwin, W. A., Bergamin, N., Sabatelli, P., Reggiani, C., Megighian, A., Merlini, L., Braghetta, P., Columbaro, M., Volpin, D., Bressan, G. M., Bernardi, P., and Bonaldo, P. (2003) Mitochondrial dysfunction and apoptosis in myopathic mice with collagen VI deficiency. *Nat. Genet.* **35**, 367–371
- Grumati, P., Coletto, L., Sabatelli, P., Cescon, M., Angelin, A., Bertaglia, E., Blaauw, B., Urciuolo, A., Tiepolo, T., Merlini, L., Maraldi, N. M., Bernardi, P., Sandri, M., and Bonaldo, P. (2010) Autophagy is defective in collagen VI muscular dystrophies, and its reactivation rescues myofiber degeneration.

## Heterogeneity of Collagen VI Microfibrils

- Nat. Med.* **16**, 1313–1320
23. Urciuolo, A., Quarta, M., Morbidoni, V., Gattazzo, F., Molon, S., Grumati, P., Montemurro, F., Tedesco, F. S., Blaauw, B., Cossu, G., Vozzi, G., Rando, T. A., and Bonaldo, P. (2013) Collagen VI regulates satellite cell self-renewal and muscle regeneration. *Nat. Commun.* **4**, 1964
  24. Beecher, N., Roseman, A. M., Jowitt, T. A., Berry, R., Troilo, H., Kammerer, R. A., Shuttleworth, C. A., Kielty, C. M., and Baldock, C. (2011) Collagen VI, conformation of A-domain arrays and microfibril architecture. *J. Biol. Chem.* **286**, 40266–40275
  25. Arnoux, B., Mériçgeau, K., Saludjian, P., Norris, F., Norris, K., Bjørn, S., Olsen, O., Petersen, L., and Ducruix, A. (1995) The 1.6 Å structure of Kunitz-type domain from the  $\alpha 3$  chain of human type VI collagen. *J. Mol. Biol.* **246**, 609–617
  26. Becker, A. K., Mikolajek, H., Paulsson, M., Wagener, R., and Werner, J. M. (2014) A structure of a collagen VI VWA domain displays N and C termini at opposite sides of the protein. *Structure* **22**, 199–208
  27. Knupp, C., and Squire, J. M. (2001) A new twist in the collagen story—the type VI segmented supercoil. *EMBO J.* **20**, 372–376
  28. Ball, S., Bella, J., Kielty, C., and Shuttleworth, A. (2003) Structural basis of type VI collagen dimer formation. *J. Biol. Chem.* **278**, 15326–15332
  29. Fitzgerald, J., Mörgelin, M., Selan, C., Wiberg, C., Keene, D. R., Lamandé, S. R., and Bateman, J. F. (2001) The N-terminal N5 subdomain of the  $\alpha 3$ (VI) chain is important for collagen VI microfibril formation. *J. Biol. Chem.* **276**, 187–193
  30. Aigner, T., Hambach, L., Söder, S., Schlötzer-Schrehardt, U., and Pöschl, E. (2002) The C5 domain of Col6A3 is cleaved off from the Col6 fibrils immediately after secretion. *Biochem. Biophys. Res. Commun.* **290**, 743–748
  31. Tooley, L. D., Zamurs, L. K., Beecher, N., Baker, N. L., Peat, R. A., Adams, N. E., Bateman, J. F., North, K. N., Baldock, C., and Lamandé, S. R. (2010) Collagen VI microfibril formation is abolished by an  $\alpha 2$ (VI) von Willibrand factor type A domain mutation in a patient with Ullrich congenital muscular dystrophy. *J. Biol. Chem.* **285**, 33567–33576
  32. Maertens, B., Hopkins, D., Franzke, C.-W., Keene, D. R., Bruckner-Tuderman, L., Greenspan, D. S., and Koch, M. (2007) Cleavage and oligomerization of gliomedin, a transmembrane collagen required for node of Ranvier formation. *J. Biol. Chem.* **282**, 10647–10659
  33. Colombatti, A., Ainger, K., and Colizzi, F. (1989) Type VI collagen: high yields of a molecule with multiple forms of  $\alpha 3$  chain from avian and human tissues. *Matrix* **9**, 177–185
  34. Peacock, A. C., and Dingman, C. W. (1968) Molecular weight estimation and separation of ribonucleic acid by electrophoresis in agarose-acrylamide composite gels. *Biochemistry* **7**, 668–674
  35. Konarev, P. V., Volkov, V. V., Sokolova, A. V., Koch, M. H. J., and Svergun, D. I. (2003) PRIMUS: a Windows PC-based system for small-angle scattering data analysis. *J. Appl. Crystallogr.* **36**, 1277–1282
  36. Blanchet, C. E., Spilotros, A., Schwemmer, F., Graewert, M. A., Kikhney, A., Jeffries, C. M., Franke, D., Mark, D., Zengerle, R., Cipriani, F., Fiedler, S., Roessle, M., and Svergun, D. I. (2015) Versatile sample environments and automation for biological solution x-ray scattering experiments at the P12 beamline (PETRA III, DESY). *J. Appl. Crystallogr.* **48**, 431–443
  37. Svergun, D. I. (1992) Determination of the regularization parameter in indirect-transform methods using perceptual criteria. *J. Appl. Crystallogr.* **25**, 495–503
  38. Svergun, D. I. (1999) Restoring low resolution structure of biological macromolecules from solution scattering using simulated annealing. *Biophys. J.* **76**, 2879–2886
  39. Volkov, V. V., and Svergun, D. I. (2003) Uniqueness of *ab initio* shape determination in small-angle scattering. *J. Appl. Crystallogr.* **36**, 860–864
  40. Petoukhov, M. V., and Svergun, D. I. (2005) Global rigid body modeling of macromolecular complexes against small-angle scattering data. *Biophys. J.* **89**, 1237–1250
  41. Tria, G., Mertens, H. D., Kachala, M., and Svergun, D. I. (2015) Advanced ensemble modelling of flexible macromolecules using x-ray solution scattering. *IUCrJ.* **2**, 207–217
  42. van Heel, M., Harauz, G., Orlova, E. V., Schmidt, R., and Schatz, M. (1996) A new generation of the IMAGIC image processing system. *J. Struct. Biol.* **116**, 17–24
  43. Spissinger, T., and Engel, J. (1995) Type VI collagen beaded microfibrils from bovine cornea depolymerize at acidic pH, and depolymerization and polymerization are not influenced by hyaluronan. *Matrix Biol.* **14**, 499–505
  44. Bober, M., Enochsson, C., Collin, M., and Mörgelin, M. (2010) Collagen VI is a subepithelial adhesive target for human respiratory tract pathogens. *J. Innate Immun.* **2**, 160–166
  45. Baschong, W., and Wrigley, N. G. (1990) Small colloidal gold conjugated to Fab fragments or to immunoglobulin G as high-resolution labels for electron microscopy: a technical overview. *J. Electron Microsc. Tech.* **14**, 313–323
  46. Roth, J., Bendayan, M., and Orci, L. (1980) FITC-protein A-gold complex for light and electron microscopic immunocytochemistry. *J. Histochem. Cytochem.* **28**, 55–57
  47. Rambo, R. P., and Tainer, J. A. (2011) Characterizing flexible and intrinsically unstructured biological macromolecules by SAS using the Porod-Debye law. *Biopolymers* **95**, 559–571
  48. Ball, S. G., Baldock, C., Kielty, C. M., and Shuttleworth, C. A. (2001) The role of the C1 and C2 a-domains in type VI collagen assembly. *J. Biol. Chem.* **276**, 7422–7430
  49. Rambo, R. P., and Tainer, J. A. (2013) Accurate assessment of mass, models and resolution by small-angle scattering. *Nature* **496**, 477–481
  50. Gebauer, J. M., Kobbe, B., Paulsson, M., and Wagener, R. (2015) Structure, evolution and expression of collagen XXVIII: lessons from the zebrafish. *Matrix Biol.* 10.1016/j.matbio.2015.07.001